

國立臺灣大學電機資訊學院資訊工程學研究所

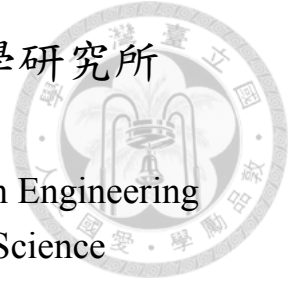
碩士論文

Graduate Institute of Computer Science and Information Engineering

College of Electrical Engineering and Computer Science

National Taiwan University

Master Thesis



IEEE 802.15.4 協定下能量收集無線感測網路之效能分析  
Modeling and Analysis of Energy Harvesting Sensor Nodes in  
IEEE 802.15.4 Protocols

陳育旋

Yu-Hsuan Chen

指導教授：逢愛君博士

Advisor: Ai-Chun Pang, Ph.D.

中華民國 105 年 6 月

June, 2016

# 致謝



因為有許多人的幫忙，這篇論文才得以完成。

首先要感謝的是我的指導教授逢愛君老師，從我大四確定要進實驗室後，老師在研究以及生活上都給予了許多的協助，包含教導我做研究的方式和應有的態度、讓不是博士生的我遠赴紐西蘭做半年的研究、以及安排我畢業後的出路，我對老師只有心中滿滿的感激。再來是我在紐西蘭做研究時的兩位教授 Winston 老師和 Bryan 老師，除了給我全額的獎學金，讓我在經濟上沒有顧慮外，老師們總是很關心我的適應狀況，而每週兩次的討論也會鼓勵我用很生硬的英文和大家分享我的研究成果，並適時的給予回應，在我回台灣後，還是定期和老師們書信往返，並且每週一次討論進度，希望我們之後的研究也可以順利，最謝謝老師們的事情是，他們讓我相信，我的想法也可以很有價值。再來是謝謝實驗室的淵耀學長、小泉學長、彥儒學長、清智學長和詩梵學姐在研究上的協助，還有不時的和大家聊天，讓實驗室的生活豐富了起來，也特別感謝學長姐在口試前兩天幫我們預演了四個小時。再來謝謝我在紐西蘭的朋友們 Hang、Liang、Gloria、Alex、Deepak、Michael、David 和 Abigail，大家中午總是圍在實驗室外的桌子吃自己帶來的午餐，聊一聊研究和生活中的趣事，讓我增長了不少對於國外和博士生活的見聞。最後要感謝我家人和小至對我的支持和幫助，讓我可以專心的完成這篇論文。

做研究就像一趟沒有終點的旅程，途中所見的風景就是最大的收穫。由衷的感謝這一路上幫助過我的所有人，謝謝。

# 中文摘要



在物聯網中，裝置的大小限制了本身能夠儲存的電量，使得網路的壽命受到影響，而藉由能量收集，讓裝置能夠自行充電，被視為一種延長網路壽命的方式。但是因為環境的影響，有別於以往用電池供電的方式，能量收集的電量大小會隨著時間變動，進而影響無線感測網路的運作，因此，以能量收集為供電方式的無線感測網路的效能需要被重新評估。在這篇論文中，我們嘗試用模型去描述使用能量採集來充電、並採用 IEEE 802.15.4 標準下的分槽式載波感測多重存取 / 碰撞避免 (CSMA/CA) 為 MAC 協定的裝置行為，並以平均充電時間、延遲和吞吐率做為效能評估的標準，我們提出的馬可夫模型成功的描述了通道競爭和充電的過程，並且比較使用不同的能量收集技術 (例如太陽能、振動能量收集等) 的裝置效能。模型會藉由模擬進行驗證，而分析出的吞吐率結果和模擬結果的誤差不會超過 6%。

關鍵字：物聯網、能量收集、IEEE 802.15.4 標準、分槽式載波感測多重存取 / 碰撞避免、馬可夫模型

# Abstract



In the Internet of Things (IoT), the size constraint of those small and embedded devices limits the network lifetime because limited energy can be stored on these devices. In recent years, energy harvesting technology has attracted increasing attention, due to its ability to extend the network lifetime significantly. However, the performance of IoT devices powered by energy harvesting sources has not been fully analyzed and understood. In this paper, we model the energy harvesting process in IoT devices using slotted Carrier Sense Multiple Access with Collision Avoidance (CSMA /CA) mechanism of IEEE 802.15.4 standard, and analyze the performance in terms of charging time, throughput and delay. Our new model successfully integrates the energy harvesting process and binary backoff process through a unified Markov chain model. Finally, the new model is validated by simulation and the throughput errors between simulation and analytical model are no more than 6%. We demonstrate the application of the model with different energy harvesting rate corresponding to different sources such as solar and vibration energy harvesters.

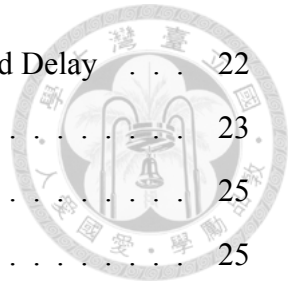
**Keywords** : Internet of Things, Energy Harvesting, IEEE 802.15.4 standard, CSMA/CA, Markov chain

# Contents



口試委員會審定書	ii
致謝	iii
中文摘要	iv
Abstract	v
Contents	vi
List of Figures	viii
List of Tables	ix
<b>1 Introduction</b>	<b>1</b>
<b>2 Related Work</b>	<b>4</b>
2.1 IEEE 802.15.4 protocol . . . . .	4
2.2 Energy Harvesting process . . . . .	4
<b>3 Overview of IEEE 802.15.4 Slotted CSMA/CA</b>	<b>6</b>
<b>4 System Model</b>	<b>8</b>
4.1 Energy harvesting process . . . . .	8
4.2 State space of the Markov model . . . . .	10
4.3 State transitions . . . . .	12
4.4 Stationary distribution . . . . .	14
4.5 Expression of Charging Time Ratio, Throughput and Delay . . . . .	20
<b>5 Model Validation</b>	<b>22</b>
5.1 Simulation Setup . . . . .	22

5.1.1	Expression of Charging Time Ratio, Throughput and Delay . . . . .	22
5.1.2	Setting of the energy harvesting rate . . . . .	23
5.2	Model Validation and Performance Analysis . . . . .	25
5.2.1	Charging Time Ratio . . . . .	25
5.2.2	Throughput . . . . .	27
5.2.3	Delay . . . . .	29
5.2.4	$E_{\min}$ and $E_{\max}$ . . . . .	32
<b>6</b>	<b>Conclusions</b>	<b>35</b>
	<b>Bibliography</b>	<b>36</b>



# List of Figures



1.1	Charging cycles of energy harvesting devices . . . . .	2
3.1	Slotted CSMA/CA mechanism with energy harvesting . . . . .	7
4.1	Markov model . . . . .	9
5.1	The assumption of each energy harvester in the simulation . . . . .	24
5.2	The charging time ratio derived from the simulation (sim) and analytical model (ana) under different parameter setting. The parameter $E_{\max} = 30$ , $q_0 = 0.3$ , $m_0 = 3$ and $m = 4$ . . . . .	26
5.3	The average throughput derived from the simulation (sim) and analytical model (ana) under different parameter setting. The parameter $E_{\max} = 30$ , $q_0 = 0.3$ , $m_0 = 3$ and $m = 4$ . . . . .	28
5.4	The average delay derived from the simulation(sim) and analytical model(ana) under different parameter setting. The parameter $E_{\max} = 30$ , $q_0 = 0.3$ , $m_0 = 3$ and $m = 4$ . . . . .	30
5.5	The performance with different value of $E_{\min}(m = 2, 3, 4, 5)$ . The parameter $E_{\max} = 30$ , $N = 20$ , $L = 7$ , $q_0 = 0.3$ , and $m_0 = 3$ . . . . .	31
5.6	The performance with different value of $E_{\max}$ . The parameter $N = 20$ , $L = 7$ , $q_0 = 0.3$ , $m_0 = 3$ and $m = 4$ . . . . .	33

# List of Tables



4.1	Symbols used to describe the System Model . . . . .	10
5.1	energy harvesting rate with 10cm <sup>2</sup> or 10cm <sup>3</sup> harvesting material . . . . .	23



# Chapter 1



## Introduction

The uses of Internet of Things(IoT) appears in a range of different domains [1] such as structural health monitoring, animal tracking and environmental surveillance. Despite the ubiquitous deployment of IoT devices, one prevailing problem with the network is the limited energy stored on each device, which can suspend the network operation without notice. Since most sensing devices are small and embedded, the energy stored in each device is limited. How to assure that each device can harvest sufficient energy for continuous operation is an important issue.

Replenishing the energy source by replacing batteries is a way to extend the network lifetime. However, in most applications it is difficult perhaps infeasible to replace the batteries because of the physical and environmental constraints. To deal with this problem, energy harvesting for IoT devices have emerged as a promising technique to prolong the network lifetime.

Energy harvesting is a technique that can make the device harvest the ambient energy by itself, which has emerged as a prominent research topic after the use of IoT appears. It can be applied in many areas. For example, we install the solar panel on the solar vehicle, so the vehicle can be powered completely by direct solar energy. In body area networks, we put the thermoelectric energy harvesting material in the self-sustaining body sensor, and the material can generate power from the difference in temperature.

Although powering IoT devices by energy harvesting technology is one of the solutions to the limited available energy, the energy availability is not always assured. In wireless network, devices sense the channel and do backoffs to alleviate the channel contention, and if the collision occurs, devices resend packets. These operations can waste many energy, and lead to a device expending all remaining energy. It has been shown [2] that the energy consuming rate is higher than the energy harvesting rate, so the sensing device only stays

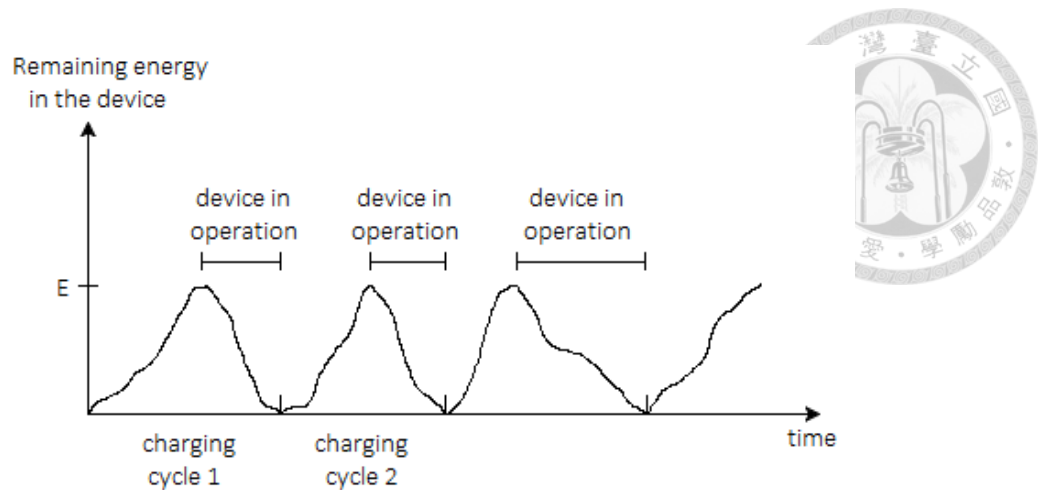


Figure 1.1: Charging cycles of energy harvesting devices

awake for a short period of time after harvesting energy. In most of the time, sensing devices cannot operate and is harvesting the energy, so the desired network performance can no longer achieved.

As illustrated in Fig. 1.1 [2], in wireless sensor networks, the energy characteristics of a node powered by energy harvesting is different from that of a node powered by batteries. For an energy harvesting node, it cannot operate until the harvested energy is accumulated to a certain level. During the node operation, if the node exhausts the energy, it stops the operation to be recharged. Since the charging cycle can be repeated, the energy harvesting device can work for a very long time without replenishing the energy source manually, but the performance is affected by the energy harvesting time.

To achieve adequate, the energy-constrained condition should be considered. Consequently, the existing Multiple Access Protocol(MAC) will not be valid under such condition. Different MAC protocols for IoT with energy harvesting are analyzed through experiments, and the result shows that the energy harvesting process directly affects the performance of network throughput via the MAC protocols [3, 4].

In this paper, we try to find out how the energy harvesting process affect the network performance. We consider the slotted Carrier Sense Multiple Access with Collision Avoidance (CSMA/CA) mechanism in IEEE 802.15.4 standard as the MAC protocol. For simplicity, we assume that the network topology is a single hop network with a star topology. We derive the expressions for charging time ratio, throughput and delay from the model,

and validate the model through simulations. Through the proposed model, we characterize the effect of energy replenishment process on the performance of IEEE 802.15.4 MAC protocol, and show the effect of energy harvesting rate on the performance.

The remainder of this paper is structured as follows. In Chapter II, we review related works. In Chapter III, we briefly describe the slotted CSMA/CA mechanism of the IEEE 802.15.4 standard, and explain how it interacts with the energy harvesting process. In Chapter IV, we propose a Markov chain model of the slotted CSMA/CA mechanism integrated with the energy harvesting process. In Chapter V, the model is validated by simulation and we compare the network performance with different energy harvesting rates. Chapter VI concludes the paper.

The contributions of this paper are: (i) a new model that integrates energy harvesting with slotted CSMA/CA mechanism of IEEE 802.15.4 standard within a unified Markov model, (ii) the energy harvesting process and the backoff process can take on different parameters, (iii) the energy consumption during binary backoff, clear channel assessment and packet transmission are necessarily distinct, and (iiii) we can successfully explain how the energy harvesting process affects the network performance. Contributions (ii) and (iii) relaxes assumptions in existing models and reflects the real-world IoT devices behaviour more closely.

# Chapter 2



## Related Work

### 2.1 IEEE 802.15.4 protocol

The IEEE 802.15.4 MAC protocol is widely adopted in IoT for example, 6LoWPAN, ZigBee and WirelessHART. It specifies the semantics for low-cost and low-power sensor networks operation. One of the access mechanisms specified by IEEE 802.15.4 standard is slotted Carrier Sense Multiple Access with Collision Avoidance (CSMA/CA) mechanism, and several simulation-based studies *e.g.*, [5–9], analyze this protocol through Markov chain models. Most of the studies are based on Bianchi’s work [10], which uses a bi-dimensional Markov chain model for IEEE 802.11 DCF.

The model developed in [6] fails to match the result, since they make the same assumption as [10] for the 802.11. The model in [5] correct this problem, but they derive the wrong probability for the channel sensing. [7] assumes that, in IEEE 802.15.4 standard, the probabilities to start channel sensing for the different devices should be independent. In [8], a packet’s retry limit is considered. In [9], in addition to the packet’s retry limit, they also consider the superframe structure of the 802.15.4 protocol. The Markov models that appear in [7–9] successfully predict the performance of the 802.15.4 protocol. However, these models assume that sensing devices have unlimited power, which limits the applicability of the model and simulation result in practical settings.

### 2.2 Energy Harvesting process

Some studies *e.g.*, [11–14], have modelled the energy replenishment (recharging) process with varying degrees of success. A favoured approach for modelling the energy replenishment is the Markovian energy model which appears in [11], [12] and [13]. The

model in [11] assumes that the packet arrival and energy replenishment are both memory-less Poisson process, and the energy state transition follows the birth and death process. A further assumption is that packet transmissions are not interrupted by the energy replenishment, which is not valid in the real energy harvesting environment, but yields insights into how throughput is affected by energy harvesting process.

To relate more realistic energy harvesting, the authors in [12] use a stochastic process to model solar and piezoelectric energy sources. The work in [12] is devoted to deriving models for optimizing energy harvesting with less attention to the interactions between protocol and energy harvesting, thus the approach therein is different.

In [13], the energy model is modelled as a Bernoulli process and is unified with the slotted CSMA/CA mechanism of the IEEE 802.11 standard. In their model, the packet length and the backoff counter freezing time are not modelled, and the energy consumption during the channel sensing state is ignored, which does not reflect changes in residual energy correctly.



# Chapter 3

## Overview of IEEE 802.15.4 Slotted CSMA/CA

In this chapter, we briefly explain the slotted CSMA/CA mechanism of the IEEE 802.15.4 standard [15], and highlight the interaction with an energy harvesting process. In the slotted CSMA/CA mechanism, there are three important variables [16] :

1. The *Number of Backoffs (NB)* is the number of times the algorithm has performed binary backoff before the packet transmission attempt. The value is initialized to 0 for a new transmission attempt.
2. The *Contention Window (CW)* is the number of backoff periods that the channel is required to be sensed idle before the transmission attempt. The value of *CW* is initialized to  $CW_0$ . If the node operation is in the Japanese 950 MHz band,  $CW_0$  shall be set to 1; otherwise,  $CW_0$  shall be set to 2.
3. The *Backoff Exponent (BE)* controls the number of backoff periods that the algorithm needs to backoff before sensing the channel. The number of backoff periods is a random variable between  $[0, 2^{BE}-1]$ .

Figure 3.1 is the flow chart of the slotted CSMA/CA mechanism with energy harvesting. First, the variables *NB* and *CW* are initialized to 0 and 2 respectively, while *BE* is initialized to  $\min(2, macMinBE)$  or *macMinBE* depending on the battery life extension(BLE). When BLE value is true, the MAC sublayer limits the random backoff exponent to ensure that the backoff duration, CCA and packet transmission is completed quickly (hence conserving energy). (**Step 1**). Next, the algorithm counts down a number of backoff periods which is randomly selected from  $[0, 2^{BE}-1]$  (**Step 2**). After counting

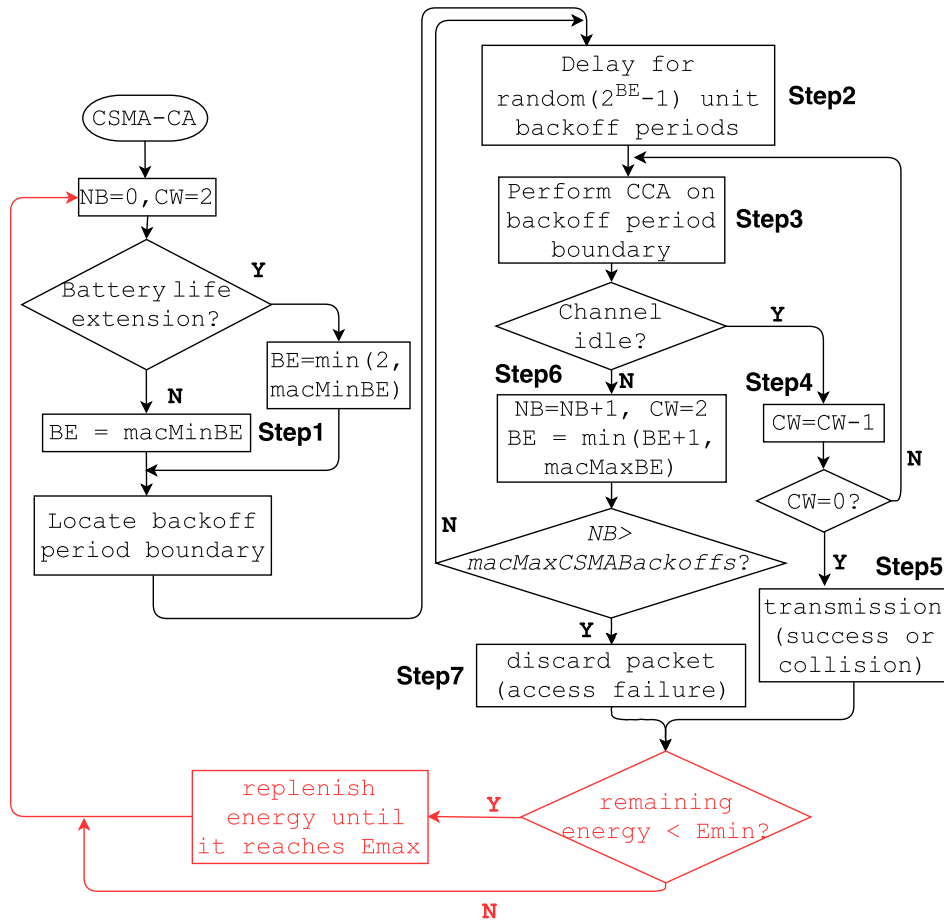


Figure 3.1: Slotted CSMA/CA mechanism with energy harvesting

down to 0, the algorithm performs Clear Channel Assessment (CCA) to check if the channel is idle (**Step 3**). If the channel is idle,  $CW$  is decreased by 1 (**Step 4**). If  $CW$  is equal to 0, the packet can be transmitted (**Step 5**), or the CCA is repeated. If the channel is sensed busy,  $NB$  is increased by 1,  $CW$  is reinitialized and  $BE$  is reinitialized to  $\min(BE+1, macMaxBE)$  (**Step 6**). If  $macMaxCSMABackoffs$  is reached, the packet is discarded (**Step 7**); otherwise, the backoff process restarts.

In this paper, we assume the MAC layer checks the remaining energy of the device after the packet transmission or access failure and this is shown in the red shaded blocks in Fig. 3.1. If the energy is below a threshold denoted by  $E_{min}$ , the energy harvesting process starts, and the energy is replenished before a new packet transmission attempt.



# Chapter 4

## System Model

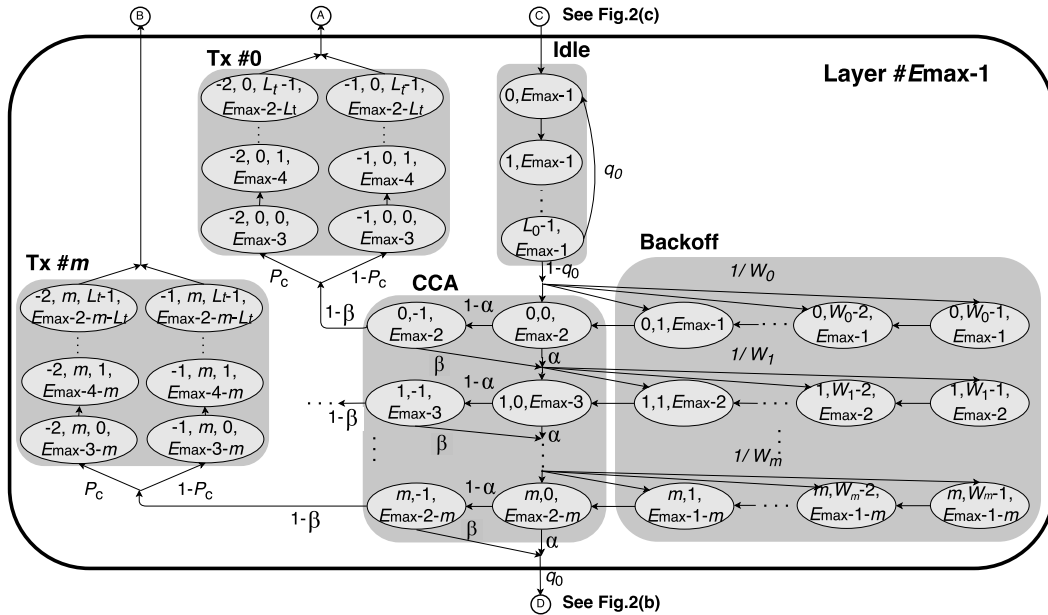
In this section, we integrate an energy harvesting process to the IEEE 802.15.4 slot-timed CSMA/CA mechanism to characterize the performance of a network of IoT devices powered by energy harvesting. We focus on a single hop star network, in which every device transmits packets to the personal area network (PAN) coordinator and receives an acknowledgement (ACK). In the model, we assume that each device has a supercapacitor to store energy, and the maximum energy capacity of the supercapacitor is  $E_{\max}$  unit.

During normal operation, defined as the MAC protocol in the following set of states: {idle, backoff, channel sensing, packet transmission}, energy is decreased. After the packet transmission process (success or collision) is finished, the device checks its remaining energy level. If the remaining energy is less than  $E_{\min}$  units, the device halts operation and enters the energy harvesting process; otherwise, the device waits for a new packet arrival.

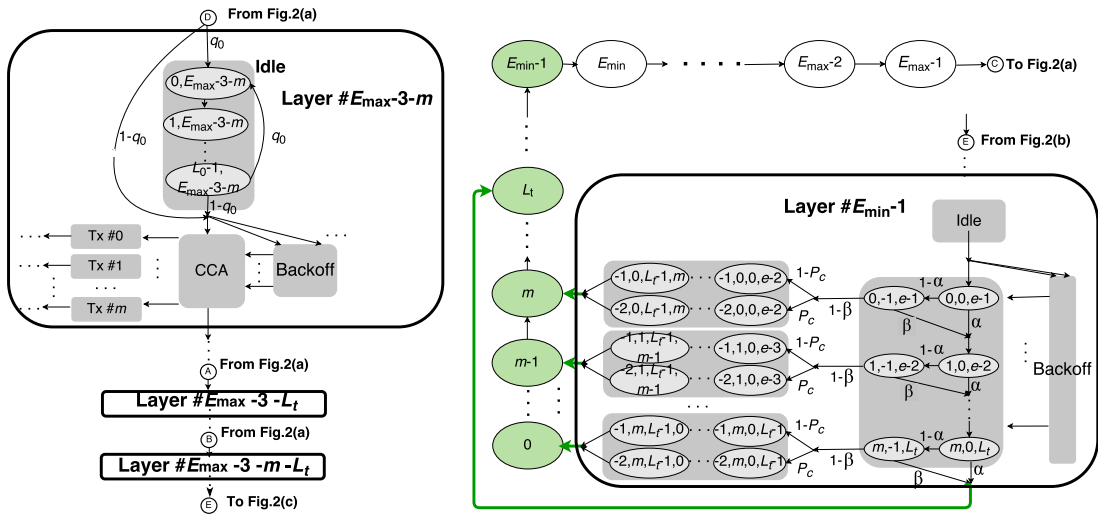
### 4.1 Energy harvesting process

Energy harvesting is the process by which ambient energy is captured and stored in the supercapacitor. We assume that the energy harvesting process follows the Poisson process to reflect the deployments of IoT in several sensor network scenarios such as structural health monitoring environments [17], bridge monitoring [18] and harvesting solar energy in situations whereby the solar irradiance is variable due to the passing of clouds [19]. The energy harvesting process stops when the energy level in the supercapacitor reaches  $E_{\max}$  and the CSMA/CA mechanism restarts operation.





(a) Transitions and states of the Markov chain model for CSMA/CA depicted as a single layer.



(b) Transitions between adjacent CSMA/CA backoff layers. This figure is connected to Fig. 4.1(a).  
 (c) Transitions and states of the energy harvesting sub-chain.

Figure 4.1: Markov model



Table 4.1: Symbols used to describe the System Model

Symbol	Description
$m_0$	$macMinBE$
$m$	$macMAXCSMABackoffs$
$W_0$	$2^{macMinBE}$
$W_i$	$2^i W_0$ , for $1 \leq i \leq m$
$E_{max}$	Maximum energy capacity of the supercapacitor
$E_{min}$	Minimum energy threshold, $L_t + (m + 1) + 1$
$L_0$	The number of idle states
$L_t$	Duration for packet transmission and receiving ACK
$P_c$	Probability that collision occurs during packet transmission
$\alpha$	Probability that the channel is busy in phase CCA1
$\beta$	Probability that the channel is busy in phase CCA2
$q_0$	Probability that the device keeps idle

## 4.2 State space of the Markov model

The Markov chain model for the IEEE 802.15.4 slotted CSMA/CA mechanism with energy harvesting is shown in Fig. 4.1. The state space is categorized into four sets of states and each set is characterized with different indices. Let  $e(t)$ ,  $f(t)$ ,  $h(t)$ ,  $s(t)$  and  $k(t)$  be stochastic processes representing the the backoff stage number, the state of the backoff counter, the residual energy level of a device, the energy harvested and the number of packets awaiting transmission at time  $t$  respectively. The tuple  $\{\delta(t), e(t), f(t), h(t)\}$  form the set of **transmission states** whereby  $\delta(t)$  is the indicator process of a successful transmission or otherwise defined in Eq.(4.1). This set of states are grouped and labelled as “Tx #0” and “Tx # $m$ ” in Fig.4.1(a).

$$\delta(t) = \begin{cases} -1 & \text{if transmission successful at time } t \\ -2 & \text{if transmission unsuccessful at time } t \end{cases} \quad (4.1)$$

Transmission states  $\{-1, i, j, s\}$  and  $\{-2, i, j, s\}$  represent the successful and collided packet transmissions respectively with the indices bounded by  $i \in [0, m]$ ,  $j \in [0, L_t - 1]$  and  $s \in [E_{max} - 2 - m - L_t, E_{max} - m - 3]$ .

The backoff process is characterised by stochastic processes  $e(t)$ ,  $f(t)$  and  $h(t)$  and

the tuple  $\{e(t), f(t), h(t)\}$  denotes the set of **backoff states** and the set of **CCA states** (these sets are labelled as “Backoff” and “Idle” in Fig. 4.1(a). Backoff states  $\{i, w, s\}$  are bounded by  $i \in [0, m], w \in [1, W_i - 1]$ , in which  $i$  is the backoff stage, and  $w$  is the backoff counter. The first phase (CCA1) and the second phase (CCA2) of the CCA are denoted by states  $\{i, 0, s\}$  and  $\{i, -1, s\}, i \in [0, m]$  respectively.

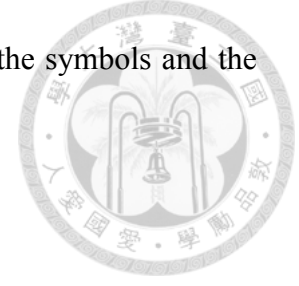
The behaviour of an idle device waiting for a new packet arrival is modelled by  $k(t)$  and  $s(t)$ , therefore the tuple  $\{k(t), s(t)\}$  denotes the set of **idle states** with the tuple defined in the range of  $\{c, s\}, c \in [0, L_0 - 1], s \in [0, E_{\max} - 1]$ . Note that the degree of traffic saturation is regulated through the parameter  $L_0$ . Finally, the energy harvesting is governed by a single process  $s(t)$  with  $s \in [0, E_{\max} - 1]$  and it forms a sub-chain shown in Fig.4.1(c).

The variable  $L_t$  denotes the number of backoff periods for packet transmission and receiving ACK and it is expressed as  $L_t = L + t_{\text{ack}} + L_{\text{ack}}$ , where  $L$  is the number of backoff periods for packet transmission,  $t_{\text{ack}}$  is the idle period between the packet transmission and receiving ACK, and  $L_{\text{ack}}$  is the number of backoff periods for receiving ACK. Based on the 802.15.4 standard specifications [15] we set  $t_{\text{ack}} = 1$  backoff period and  $L_{\text{ack}} = 2$  backoff periods. Throughout this paper, we assume that the duration for successful packet transmission and the duration for collided packet transmission are identical.

Recall that the states  $s \in [0, E_{\max} - 1]$  are energy harvesting states with  $s$  representing the residual energy level of the device, and the energy harvesting is governed by a Poisson process with rate  $\lambda$ . The value of  $\lambda$  dictates the energy units harvested in a backoff period. According to the energy consumption rates in different states, we assume that there is no energy consumption in backoff states [7]. In our model, idle states collectively consume one unit of energy, thus CCA1 and CCA2 together consume one unit energy, and each of the transmission state consumes one unit of energy. The value of  $E_{\min}$  is the sum of the energy consumed during packet transmission, the total number of backoff stages, and the energy consumed in idle states, thus:

$$E_{\min} = L_t + (m + 1) + 1. \quad (4.2)$$

In Fig. 4.1(c), the constant  $e$  is equal to  $E_{\min} - 1$ . Table 4.1 lists the symbols and the meanings in the context of the Markov model.



### 4.3 State transitions

Our model in Fig. 4.1 is composed of layers, and these layers are linked to energy harvesting states. Each layer has the same structure in terms of states and transitions. When a device terminates packet transmission and the remaining energy level  $s$  is greater than  $E_{\min}$ , the device transits to the idle state in another layer with probability  $q_0$ , or transits to the backoff state with probability  $1 - q_0$ . But if  $s$  is less than  $E_{\min}$  unit, the device transits to the energy harvesting state. For example, if the packet transmission is done in the state  $(-1, 0, L_t - 1, E_{\max} - 2 - L_t)$  and  $(E_{\max} - 2 - L_t)$  is greater than  $E_{\min}$ , the state of the device transits to the idle state  $(0, (E_{\max} - 2 - L_t) - 1)$  with probability  $q_0$ .

The index of a layer models the remaining energy level of the device when in idle states and this index is an integer defined over the range of  $E_{\min} - 1$  to  $E_{\max} - 1$ . In energy harvesting states, the permissible state transitions are shaded (green in Fig. 4.1(c)) and the sojourn time of energy harvesting states follows an exponential distribution.

Using simplified notation  $\Pr\{\mathcal{E}\}$  where  $\mathcal{E}$  denotes a transition event of the MAC, the non-null state transition probabilities of the Markov chain are:

$$\begin{aligned} & \Pr\{\text{harvesting one unit of energy}\} \\ & = P(s + 1|s) = e^{-\lambda}, \quad \text{for } 0 \leq s < E_{\max} - 1, \end{aligned} \quad (4.3)$$

$$\begin{aligned} & \Pr\{\text{transit to the first backoff stage from an idle state}\} \\ & = P(0, w, s|L_0, s) \\ & = P(0, 0, s - 1|L_0, s) \\ & = \frac{1 - q_0}{W_0}, \quad \text{for } 1 \leq w < W_0, \end{aligned} \quad (4.4)$$



$$\begin{aligned}
& \Pr\{\text{the decrement of the backoff counter}\} \\
&= P(i, w - 1, s|i, w, s) \\
&= P(i, 0, s - 1|i, 1, s) \\
&= 1, \quad \text{for } 0 \leq i \leq m \text{ and } 1 < w < W_0,
\end{aligned} \tag{4.5}$$

$$\begin{aligned}
& \Pr\{\text{new backoff after channel sensed busy during CCA1 or CCA2}\} \\
&= P(i, w, s|i - 1, 0, s) \\
&= P(i, 0, s - 1|i - 1, 0, s) \\
&= \frac{\alpha + (1 - \alpha)\beta}{W_i}, \quad \text{for } 1 \leq i \leq m \text{ and } 1 \leq w < W_i,
\end{aligned} \tag{4.6}$$

$$\begin{aligned}
& \Pr\{\text{channel is idle during CCA1 and CCA2 upon a successful packet transmission}\} \\
&= P(-1, i, 0, s - 1|i, 0, s) \\
&= (1 - \alpha)(1 - \beta)(1 - P_c),
\end{aligned} \tag{4.7}$$

$$\begin{aligned}
& \Pr\{\text{channel is idle during CCA1 and CCA2 after a collision}\} \\
&= P(-2, i, 0, s - 1|i, 0, s) \\
&= (1 - \alpha)(1 - \beta)P_c.
\end{aligned} \tag{4.8}$$

The probability that the device is in the wait state (awaiting packet arrivals) or is charged after the transmission is denoted by Eq. (4.9) and Eq. (4.10) respectively. Therefore, the non-null transition probabilities are:

$$\begin{aligned}
& \Pr\{\text{waiting state after a packet transmission}\} \\
&= P(0, s - 1| - 1, i, L_t - 1, s) \\
&= P(0, s - 1| - 2, i, L_t - 1, s) = \begin{cases} q_0, & \text{if } s \geq E_{\min} \\ 0, & \text{if } s < E_{\min} \end{cases},
\end{aligned} \tag{4.9}$$

$$\begin{aligned}
& \Pr\{\text{energy harvesting after the packet transmission}\} \\
&= P(s | -1, i, L_t - 1, s) \\
&= P(s | -2, i, L_t - 1, s) = \begin{cases} 0, & \text{if } s \geq E_{\min} \\ 1, & \text{if } s < E_{\min} \end{cases}. \tag{4.10}
\end{aligned}$$



If the remaining energy level is below  $E_{\min}$ , the device halts normal operation and the energy harvesting process starts. Subsequently, the probability that the device is in a wait state (awaiting packet arrival) or is charged after the access failure is given by Eq. (4.11) and Eq. (4.12). The device waits for a new packet arrival only if the remaining energy level is above  $E_{\min}$ . Thus, the non-null transition probabilities are:

$$\begin{aligned}
& \Pr\{\text{waiting state after an access failure}\} \\
&= P(0, s - 1 | m, 0, s) \\
&= \begin{cases} q_0 \times (\alpha + (1 - \alpha)\beta), & \text{if } s \geq E_{\min} \\ 0, & \text{if } s < E_{\min} \end{cases}, \tag{4.11}
\end{aligned}$$

$$\begin{aligned}
& \Pr\{\text{energy harvesting after the access failure}\} \\
&= P(s | m, 0, s) = \begin{cases} 0, & \text{if } s \geq E_{\min} \\ \alpha + (1 - \alpha)\beta, & \text{if } s < E_{\min} \end{cases}. \tag{4.12}
\end{aligned}$$

## 4.4 Stationary distribution

The stationary distribution of the embedded Markov chain of Fig. 4.1 is a vector  $\pi$ . For ease of presentation, we decompose the vector into four different states:

- **idle states**, the stationary probability is

$$\pi_{c,s}, c \in (0, L_0 - 1), s \in (E_{\min} - 1, E_{\max} - 1),$$



- **backoff / CCA states**, the stationary probability is

$$\pi_{i,w,s}, i \in (0, m), w \in (-1, W_i - 1),$$

- **packet transmission states**, the stationary probability is

$$\pi_{-1,i,j,s} \text{ and } \pi_{-2,i,j,s}, i \in (0, m), j \in (0, L_t - 1),$$

- **energy harvesting states**, the stationary probability is

$$\pi_s, s \in (0, E_{\max} - 1),$$

such that

$$\boldsymbol{\pi} = (\pi_{c,s} \cup \pi_{i,w,s} \cup \pi_{-1,i,j,s} \cup \pi_{-2,i,j,s} \cup \pi_s).$$

Using this notation, the transition probabilities that appear earlier in Eq. (4.4) and Eq. (4.5) are simplified to:

$$\pi_{i,w,s+1} = \frac{W_i - w}{W_i} \pi_{i,0,s}, \quad (4.13)$$

where  $w$  is from 1 to  $W_i - 1$ . Similarly, the transition probabilities in Eq. (4.6) are expressed as

$$\pi_{i,0,s-i} = (\alpha + (1 - \alpha)\beta)^i \pi_{0,0,s}. \quad (4.14)$$

Summing the state probabilities for a layer indexed by  $s$  (i.e. Eq. (4.4) - (4.8), Eq. (4.13) and Eq. (4.14)), we obtain the probability the Markov chain is in layer  $s$ :

$$\begin{aligned} & L_0 \times \pi_{0,s} + \frac{\pi_{0,0,s-1}}{2} \left( \frac{1 - (2x)^{m+1}}{1 - 2x} W_0 + \frac{1 - x^{m+1}}{1 - x} \right) \\ & + (1 - \alpha) \frac{1 - x^{m+1}}{1 - x} \pi_{0,0,s-1} + L_t (1 - x^{m+1}) \pi_{0,0,s-1} \\ & = \pi_{0,s} \times L_0 + \pi_{0,0,s-1} \times \\ & \left\{ \frac{1 - (2x)^{m+1}}{2(1 - 2x)} W_0 + \frac{1 - x^{m+1}}{1 - x} \left[ \frac{3}{2} - \alpha + (1 - x)L_t \right] \right\}, \quad (4.15) \end{aligned}$$



where  $x = \alpha + (1 - \alpha)\beta$ .

From Eq. (4.15) we expand the expressions for  $\pi_{0,s}$  and  $\pi_{0,0,s-1}$  and this yields:

$$\pi_{0,s} = \begin{cases} \frac{\pi_{E_{\max}-1}}{1-q_0}, & \text{if } s = E_{\max} - 1 \\ \frac{q_0(Q_a(s)+Q_b(s))}{1-q_0}, & \text{otherwise} \end{cases}, \quad (4.16)$$

and  $\pi_{0,0,s-1}$  is given by:

$$\pi_{0,0,s-1} = \begin{cases} (1 - q_0)\pi_{0,s}, & \text{if } s = E_{\max} - 1 \\ (1 - q_0)(Q_a(s) + Q_b(s) + \pi_{0,s}), & \text{otherwise} \end{cases}, \quad (4.17)$$

where  $Q_a(s)$  is the state transition probability to layer  $s$  due to the packet transmission and  $Q_b(s)$  is the state transition probability to  $s$  conditioned on access failure. Using Eq. (4.16) and Eq. (4.17), we establish the relationship between  $\pi_{0,s}$  and  $\pi_{0,0,s-1}$  which expresses the probability the Markov chain is in state  $s$  (Eq. (4.15)) as a function of  $\pi_{0,s}$ .

The derivation of  $Q_a(s)$  is as follows: we introduce the auxiliary variable  $r = (s + 1) + L_t$ , to denote the remaining energy level of the device during its successful CCA1 and CCA2. For  $r + 1 > E_{\max} - 1$ , the corresponding  $Q_a(s)$  is 0, while for  $r + 1 \leq E_{\max} - 1$ , we obtain  $Q_a(s)$  as:

$$\begin{aligned} Q_a(s) &= \sum_{i=(r+1)+0}^n (1 - \alpha)(1 - \beta)\pi_{i-(r+1),0,r} \\ &= \sum_{i=(r+1)+0}^n (1 - \alpha)(1 - \beta)x^{i-(r+1)}\pi_{0,0,i-1}, \end{aligned}$$

where  $(r + 1)$  and  $n = \min(E_{\max} - 1, (r + 1) + m)$  are the respective minimum and maximum index of layers that the state transition from these layers to state  $(0, s)$  after the packet transmission exists. This relationship is direct from Eq. (4.7) and Eq. (4.8).



Moreover, from Eq. (4.11), the expression for  $Q_b(s)$  is readily obtained as:

$$Q_b(s) = \begin{cases} 0, & \text{if } d > E_{\max} - 1 \\ x \times \pi_{m,0,s+1}, & \text{if } d \leq E_{\max} - 1 \end{cases}, \quad (4.18)$$



where  $d = (s + 1) + m + 1$ , which is the index of the layer and the state transition from the layer to state  $(0, s)$  after an access failure. When  $d \leq E_{\max} - 1$ , the probability the Markov chain transits to state  $s$  can be rewritten as follows:

$$Q_b(s) = x \times \pi_{m,0,s+1} = x^{m+1} \pi_{0,0,d-1}.$$

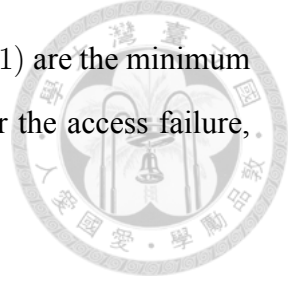
Now, we will derive the stationary distribution expressions for the energy harvesting states  $\pi_s, s \in (0, E_{\max} - 1)$ . Starting from the expressions in Eq. (4.3), Eq. (4.10) and Eq. (4.12), we have:

$$\pi_s = \begin{cases} R_a(s) + R_b(s), & \text{if } s = 0 \\ R_a(s) + R_b(s) + \pi_{s-1}, & \text{if } 0 < s \leq E_{\min} - 1 \\ \pi_{E_{\min}-1}, & \text{if } E_{\min} - 1 < s \end{cases} \quad (4.19)$$

where  $R_a(s)$  is the probability that the device starts energy harvesting process with remaining energy level  $s$  after the packet transmission, and  $R_b(s)$  is the probability that the device starts energy harvesting process with remaining energy level  $s$  after the access failure.

The derivation of  $R_a(s)$  is similar to that of  $Q_a(s)$ . Denote the remaining energy level of the device during its successful CCA1 and CCA2 by  $u$  such that  $u = s + L_t$ . When  $u + 1 > E_{\max} - 1$ , the value of  $R_a(s)$  is 0. When  $u + 1 \leq E_{\max} - 1$ , the expression of  $R_a(s)$  is

$$\begin{aligned} R_a(s) &= \sum_{i=v}^k (1 - \alpha)(1 - \beta) \pi_{i-(u+1),0,u} \\ &= \sum_{i=v}^k (1 - \alpha)(1 - \beta) x^{i-(u+1)} \pi_{0,0,i-1}, \end{aligned} \quad (4.20)$$



where  $v = \max(u + 1, E_{\min} - 1)$  and  $k = \min((u + 1) + m, E_{\max} - 1)$  are the minimum and maximum index of those layers that can transit to state  $(s)$  after the access failure, respectively. The expression of  $R_b(s)$  is

$$R_b(s) = \begin{cases} 0, & \text{if } s + m + 1 < E_{\min} - 1 \\ 0, & \text{if } s + m + 1 > E_{\max} - 1 \\ x \times \pi_{m,0,s}, & \text{if } E_{\max} - 1 \geq s + m + 1 \geq E_{\min} - 1 \end{cases}. \quad (4.21)$$

When  $s + m + 1 \geq E_{\min} - 1$ , we can rewrite  $R_b(s)$  as

$$x \times \pi_{m,0,s} = x^{m+1} \pi_{0,0,s+m}$$

The probability of each state in Eq. (4.15) - (4.21) can be rewritten as a function of  $\pi_{0,0,s-1}$ ,  $s \in (E_{\min} - 1, E_{\max} - 1)$ . Given that we have derived the relations of  $\pi_{0,s}$  and  $\pi_{0,0,s-1}$ , the sum of the stationary probability of Markov chain can further be expressed by  $\pi_{0,E_{\max}-1}$ .

We now derive the remaining unknowns  $\alpha$ ,  $\beta$  and  $P_c$  by considering the sojourn time of the states. Let  $\mathbf{P}$  be the limiting probability of the Markov chain in Fig. 4.1. For CCA1 states, the limiting probability  $P_{i,0,s}$  and its relationship with  $\pi_{i,0,s}$  is given by:

$$P_{i,0,s} = \lim_{t \rightarrow \infty} P_{i,0,s}(t) = \frac{\pi_{i,0,s} E(T_{i,0,s})}{\sum_{k \in S} \pi_k E(T_k)},$$

where  $T_k$  is the sojourn time of state  $k$ , and  $S$  presents a set of discrete states of the Markov chain. Because the sojourn time of each state in each layer is normalized to a unit backoff period, and the sojourn time of energy harvesting states depends only on the harvesting rate  $\lambda$ , the limiting probability of CCA1 states is readily expressed as a function of  $\pi_{0,E_{\max}-1}$ .

Next, we introduce a probability  $\tau$  that the device performs its CCA1 in a random back-off period, which is equal to the sum of the limiting probability of CCA1 states. Similar to [8], the value of  $\tau$  is given by

$$\tau = \sum_{s=E_{\min}-2}^{E_{\max}-2} \frac{1 - x^{m+1}}{1 - x} P_{0,0,s}. \quad (4.22)$$

Now, we can derive the probabilities  $\alpha$ ,  $\beta$  and  $P_c$ . The conditional collision probability  $P_c$  is the probability that the collision occurs during packet transmission. In the slotted CSMA/CA mechanism, a collision occurs only if at least one of the remaining  $N - 1$  devices start packet transmission in a same backoff period. Hence,  $P_c$  is

$$P_c = 1 - (1 - \tau)^{N-1}, \quad (4.23)$$

where  $N$  is the number of nodes.

The probabilities  $\alpha$  and  $\beta$  are the probabilities that the channel is sensed busy during CCA1 and CCA2:

$$\alpha = \alpha_1 + \alpha_2, \quad (4.24)$$

where  $\alpha_1$  is the probability that the channel is sensed busy during CCA1 due to the packet transmission (the proof of (4.24) appears in [7] and [8].) Since the probability that a device starts to transmit a packet is  $\tau(1 - \alpha)(1 - \beta)$ , and  $1 - (1 - \tau)^{N-1}$  is the probability that at least one of the  $N - 1$  remaining devices stay in CCA1 states,  $\alpha_1$  is

$$\alpha_1 = L(1 - (1 - \tau)^{N-1})(1 - \alpha)(1 - \beta)$$

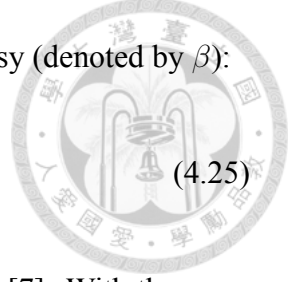
and  $\alpha_2$  is the probability that the channel is sensed busy during CCA1 due to ACK transmission, which is expressed as:

$$\begin{aligned} \alpha_2 &= L_{ack} \frac{N\tau(1 - \tau)^{N-1}(1 - \alpha)(1 - \beta)}{(1 - (1 - \tau)^N)(1 - \alpha)(1 - \beta)} \\ &\quad \times (1 - (1 - \tau)^{N-1})(1 - \alpha)(1 - \beta) \\ &= L_{ack} \frac{N\tau(1 - \tau)^{N-1}}{1 - (1 - \tau)^N} (1 - (1 - \tau)^{N-1})(1 - \alpha)(1 - \beta), \end{aligned}$$

where  $(1 - (1 - \tau)^N)(1 - \alpha)(1 - \beta)$  is the probability that at least one device can transmit a packet, and  $N\tau(1 - \tau)^{N-1}(1 - \alpha)(1 - \beta)$  is the probability that only one device is

transmitting the packet. The probability that the channel is sensed busy (denoted by  $\beta$ ):

$$\beta = \frac{1 - (1 - \tau)^{N-1} + N\tau(1 - \tau)^{N-1}}{2 - (1 - \tau)^N + N\tau(1 - \tau)^{N-1}}. \quad (4.25)$$



Further details about deriving the probabilities  $\alpha$ ,  $\beta$  and  $P_c$  appear in [7]. With the complete characterization of these transition probabilities, the model is solved numerically.

## 4.5 Expression of Charging Time Ratio, Throughput and Delay

In this section, we try to derive the expression of charging time, throughput and delay from the proposed model.

Charging time ratio is the ratio of the energy harvesting time to the device's whole system time, and the whole system time is the energy harvesting time plus the CSMA/CA operation time. For example, if charging time ratio = 0.6, it means that in 10 minutes, the device will take 6 minutes to capture the ambient energy and take 4 minutes to perform the CSMA/CA operation. The average charging time ratio is derived by the following expression:

$$\begin{aligned} & \text{Charging time ratio(ana)} \\ &= \frac{\text{energy harvesting time}}{\text{energy harvesting time} + \text{CSMA/CA operation time}} \\ &= \frac{\sum_{s=0}^{E_{\max}-1} \pi_s E(T_s)}{\sum_{k \in S} \pi_k E(T_k)}, \end{aligned}$$

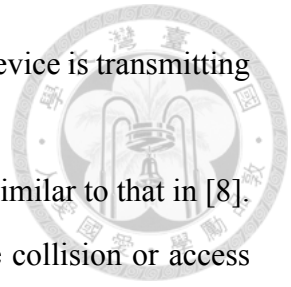
in which  $T_k$  is the sojourn time of state  $k$ , and  $S$  represents a set of discrete states of the Markov chain.

Next, we derive the average throughput. Similarly to [7], The average throughput from our analytical model is equal to:

$$\text{Throughput(ana)} = LN\tau(1 - \tau)^{N-1}(1 - \alpha)(1 - \beta)$$

where  $N\tau(1-\tau)^{N-1}(1-\alpha)(1-\beta)$  is the probability that only one device is transmitting the packet.

The derivation of the average delay from the analytical model is similar to that in [8]. However, in our model, we assume that the packet is dropped if the collision or access failure occurs, so  $macMaxFrameRetries = 0$ .



# Chapter 5



## Model Validation

In this chapter, we validate the proposed model by simulation, and analyze the performance in terms of charging time, throughput and delay. The simulation is developed in Matlab.

### 5.1 Simulation Setup

The algorithm follows the pseudo code proposed in [7] and we extend it to accommodate acknowledgements and the unsaturated traffic conditions. Because the device only changes state at the backoff period boundaries, we normalize the simulation step to one backoff period. The total simulation time is  $10^8$  backoff periods.

For the probability  $q_0$ , we generate a uniform random number between 0 and 1. If the number is not bigger than  $q_0$ , the device remains idle, otherwise it starts the backoff process. The size of the backoff counter is a randomly chosen integer between 0 to  $2^{BE} - 1$ .

#### 5.1.1 Expression of Charging Time Ratio, Throughput and Delay

The average charging time for each device is:

$$\text{Charging time ratio(sim)} = \frac{T_{\text{charging}}}{N \times T_{\text{simulation}}}$$

where  $T_{\text{charging}}$  denotes the sum of devices' energy harvesting time. The average throughput from the simulation is simply:

$$\text{Throughput(sim)} = \frac{n_s \times L}{T_{\text{simulation}}}$$

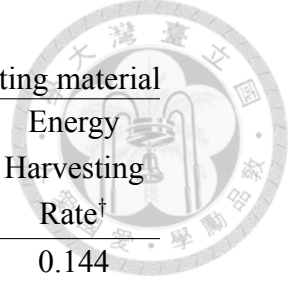


Table 5.1: energy harvesting rate with 10cm<sup>2</sup> or 10cm<sup>3</sup> harvesting material

Material	Power Density ( $\mu\text{W}/\text{cm}^2$ )	Energy Harvesting Rate (mW)	Energy Harvesting Rate <sup>†</sup>
Electromagnetic [20]	433 <sup>**</sup>	4.33	0.144
Piezoelectric [21]	106.9 <sup>**</sup>	1.069	0.0356
Electrostatic (Triboelectric) [22]	0.648	0.0064	0.0002
Thermoelectric [23]	60	0.6	0.02
Solar - direct sunlight [24]	8000	80	2.66

<sup>†</sup> the energy units harvested in a backoff period

<sup>\*\*</sup> unit is  $\mu\text{W}/\text{cm}^3$

where  $n_s$  denotes the number of successfully transmitted packets, and  $T_{\text{simulation}}$  refers to the total simulation time. The unit of the packet length  $L$  and the unit of simulation time are both a backoff period.

Next, we derive the average delay. We define the average delay of a packet as the time from the first attempt of backoff, until the time when the ACK is received. Consistent with the analytical model, we do not consider the delay of discarded packets due to the collision or access failure. The expression of the average delay is as follows:

$$\text{Delay}(\text{sim}) = \frac{T_{\text{delay}}}{n_s} \times T$$

where  $T_{\text{delay}}$  denotes the sum of packets' delay while  $T$  is the length of the backoff period. According to IEEE 802.15.4 standard [15], a backoff period is 20 symbols long (*aUnitBackoffPeriod*), and 1 symbol is 4 bits. For a typical bit rate of 250kbps,  $T$  is  $\frac{80\text{bits}}{250\text{kbps}} = 0.32\text{ms}$ .

### 5.1.2 Setting of the energy harvesting rate

The energy harvesting rates from different energy harvesting technologies with dimension 10cm<sup>2</sup> or 10cm<sup>3</sup> is listed in Table 5.1. In [20], they harvested energy through an electromagnetic transducer constructed with two permanent magnets and a 11cm<sup>3</sup> coil. Output power of 4.33mW is achieved with a 90 $\Omega$  load resistor connected to the transducer.

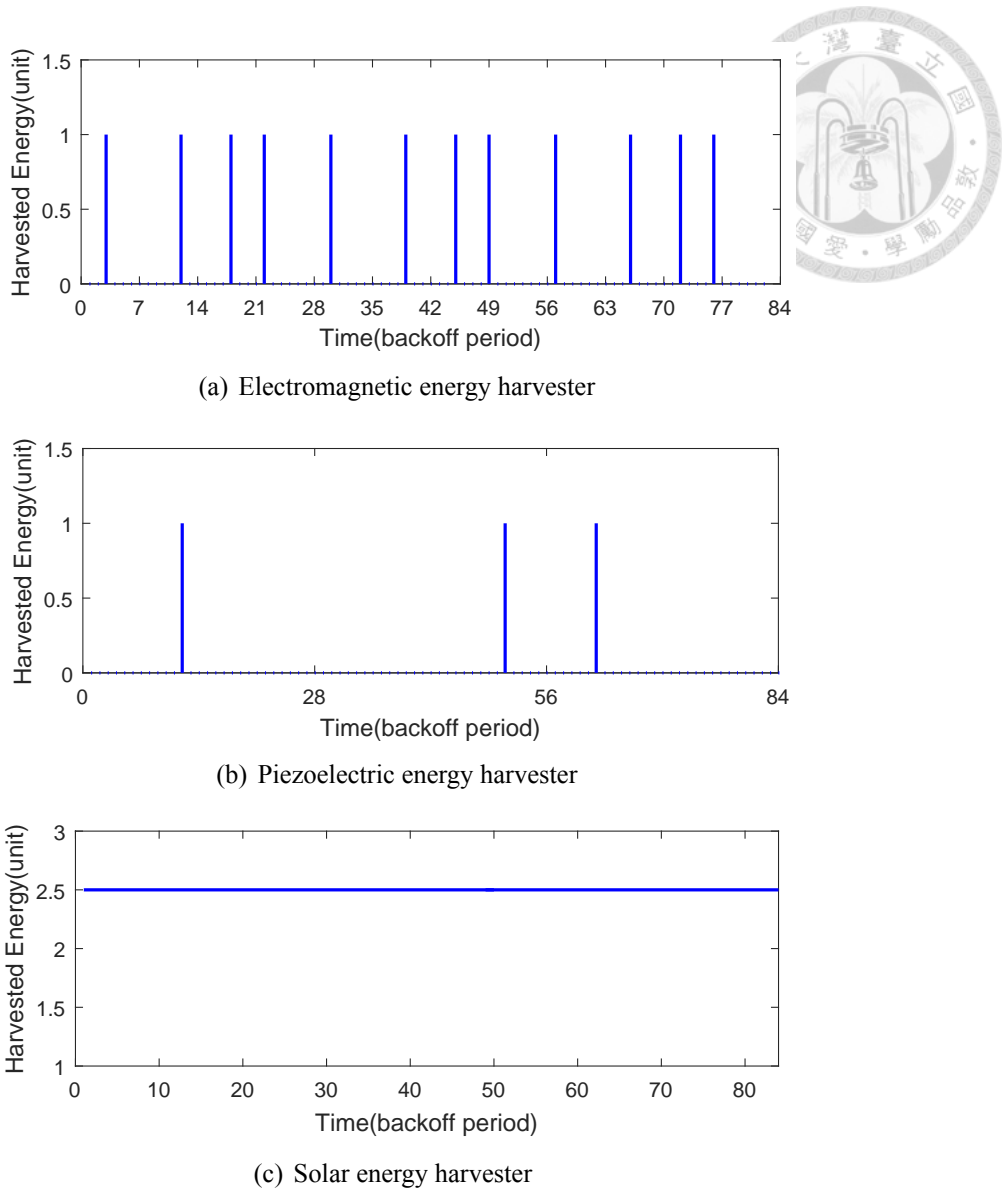


Figure 5.1: The assumption of each energy harvester in the simulation

In [21], the energy is harvested using piezoelectric bimorph/magnet composites and an AC power line. When the power is switched on, the AC magnetic field interacts with the magnetization of the magnet inciting the piezoelectric cantilever. In [22], they implement the electrodes, diode ladder circuit and a energy harvesting circuit on skirt paddles. Due to the triboelectric effect, these paddles generate electrostatic energy when brushed rapidly against each other. In [23], they wear the  $9\text{cm}^2$  thermoelectric energy harvester on the wrist. Using the temperature difference between the skin and ambient temperature, the thermoelectric energy is generated. The maximum generated power is about  $60\mu\text{W}/\text{cm}^2$  indoors and about  $600\mu\text{W}/\text{cm}^2$  at a temperature of  $0^\circ\text{C}$ . In [24], the National Institute of



Water and Atmospheric Research(NIWA) conducts the SolarView calculation for a year in Kelburn, Wellington. The lowest harvested Solar Energy during daylight is 80mW.

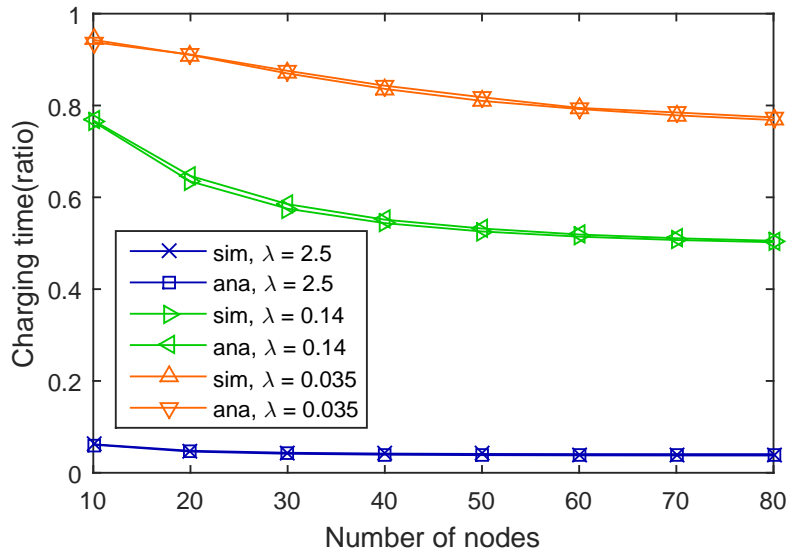
In this paper, we assume that the energy consumption rate for packet transmission is 30mW [8], and the actual length of a backoff period is 0.32ms. Using this relationship, the energy harvesting rate from mW is easily converted to the energy unit per backoff period and this is used to tabulate the harvesting rate in the fourth column of Table 5.1. In the paper, we choose the harvesting rate  $\lambda = 2.5, 0.14, 0.035$  as the simulation parameter, in which the rate = 2.5 is close to the rate given by outdoor solar energy harvesters, the rate = 0.14 is close to the rate given by electromagnetic energy harvesters, and rate = 0.035 is close to the rate given by piezoelectric energy harvesters.

In the simulation, we assume that each energy harvesting process follows different distribution. Since electromagnetic energy and piezoelectric energy are both the energy of vibrations, we suppose that the vibration occurs once in each cycle time, and we can harvest 1 unit of the energy when the vibration occurs. As shown in Fig. 5.1(a), for the electromagnetic energy harvester, we assume that the vibration occurs once every 7 back-off periods ( $1/7 \approx 0.14$ ). For the piezoelectric energy harvester, as shown in Fig. 5.1(b), the vibration occurs once every 28 backoff periods ( $1/28 \approx 0.035$ ). For the solar energy harvester, since the change of the solar energy harvesting rate is slow, in Fig. 5.1(c), the amount of harvested energy in each backoff period is a constant.

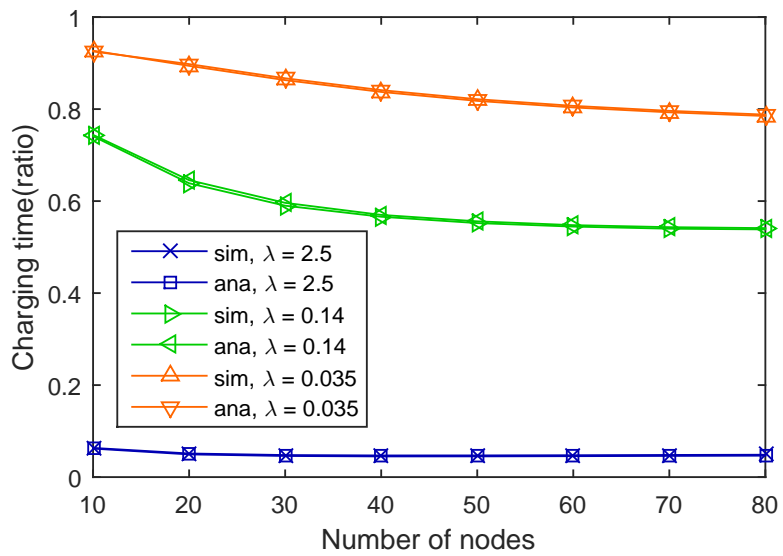
## 5.2 Model Validation and Performance Analysis

### 5.2.1 Charging Time Ratio

In Fig 5.2, we compare the charging time ratio derived from the simulation and our analytical model. The analytical model matches the simulation result closely. Subsequently, we analyze the charging time ratio of the network under different energy harvesting rate  $\lambda$ . The energy harvesting rate is the average unit of the energy harvested in one backoff period. It should be noted that the evaluation is also carried out under reasonable heavy traffic (i.e.  $q_0 = 0.3$ ).

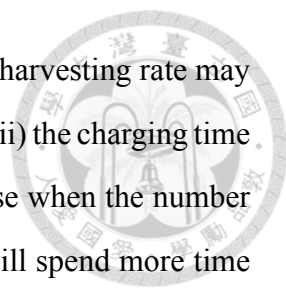


(a)  $E_{\min} = 16 (L = 7)$



(b)  $E_{\min} = 11 (L = 2)$

Figure 5.2: The charging time ratio derived from the simulation (sim) and analytical model (ana) under different parameter setting. The parameter  $E_{\max} = 30$ ,  $q_0 = 0.3$ ,  $m_0 = 3$  and  $m = 4$



From Fig 5.2(a), we can see that (i) the device with lower energy harvesting rate may spend more time on replenishing the energy. We also can find out that (ii) the charging time ratio decreases when the number of devices increases. This is because when the number of devices increases, the channel access is harder, and each device will spend more time in backoff states to wait for the next channel access.

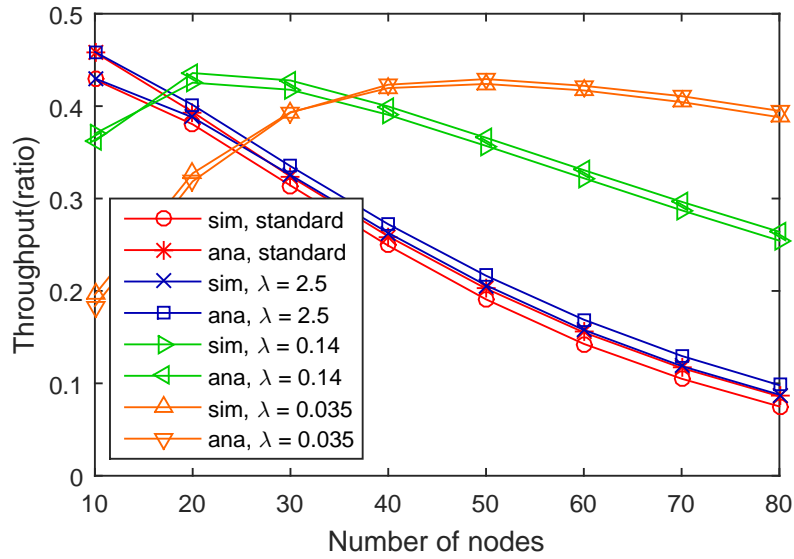
But the effect of the number of devices on the charging time ratio is not clear when the energy harvesting rate  $\lambda = 2.5$ . To explain this, we can see Fig 5.3(a). From Fig 5.3(a), we know that for the energy harvesting rate = 2.5, the network can reach the maximum throughput when the number of devices = 10, which means that the channel contention is already saturated. That is why the average charging time will not be changed when we increase the number of devices.

Now we compare Fig 5.2(a) and Fig 5.2(b). In Fig 5.2(b), we change the packet size  $L$  from 7 to 2, and from the equation of  $E_{min}$  (Eq. 4.2), the value of  $E_{min}$  is decreased too. If the number of devices and the energy harvesting rate are fixed, smaller value of  $E_{min}$  will increase the device operation time and the energy harvesting time simultaneously, so the average charging time ratio will not be changed.

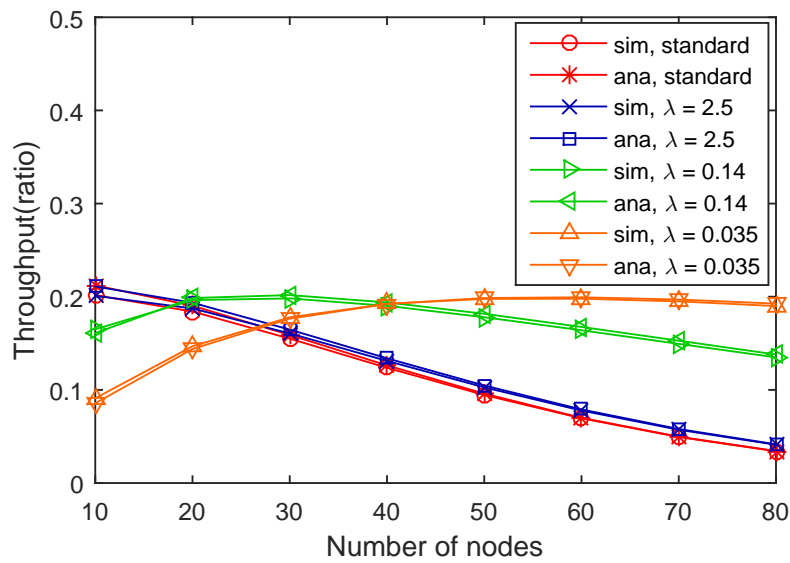
## 5.2.2 Throughput

Fig. 5.3 compares the average throughput derived from the simulation and our analytical model. In our results, the curves/points labelled “standard” refer to the basic IEEE 802.15.4 protocol in which the devices have no energy constraint (i.e. no energy harvesting state in the model). The analytical model and the simulation result match quite well. But for the smaller number of devices, the model’s result is slightly different from the simulation. This is because the derivation of  $\beta$  is more accurate for large number of devices. For further details, please refer to [7].

From the performance evaluation: (i) the throughput of the network with solar energy harvesting sources ( $\lambda = 2.5$ ) is almost equal to the throughput of network without energy constraint, and (ii) a higher energy harvesting rate yields a lower throughput. For the solar energy harvester, devices need less time replenishing the energy, so the performance is

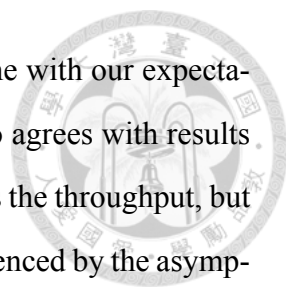


(a)  $E_{\min} = 16(L = 7)$



(b)  $E_{\min} = 11(L = 2)$

Figure 5.3: The average throughput derived from the simulation (sim) and analytical model (ana) under different parameter setting. The parameter  $E_{\max} = 30$ ,  $q_0 = 0.3$ ,  $m_0 = 3$  and  $m = 4$



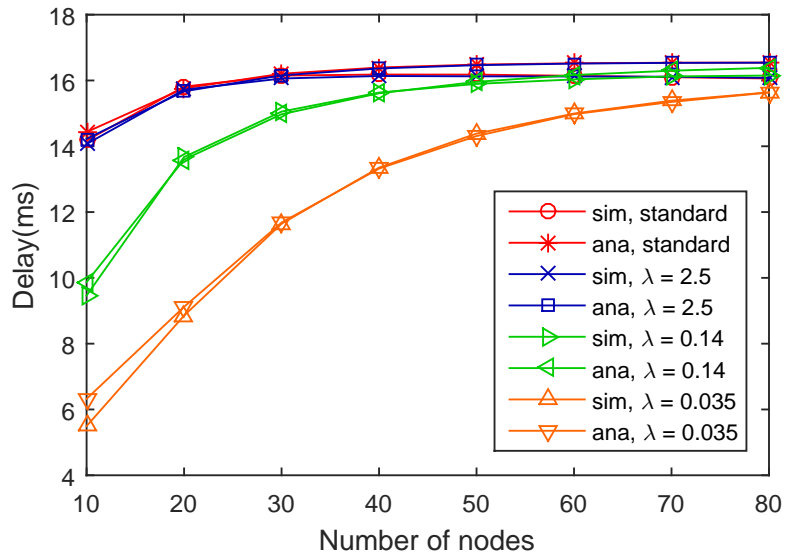
close to the performance of network without energy constraint. In line with our expectations, there is an upper bound on the throughput. Our evaluation also agrees with results from previous studies that show that energy harvesting directly affects the throughput, but our results go one step further and show that it is range bound (as evidenced by the asymptotic levelling of throughput). The reasoning behind the better performance is that energy harvesting nodes introduce lesser contention because of their intermittent transmission attempts which essentially reduces the overall attempts on the channel. It is well known that CSMA protocols suffer throughput degradation when large number of nodes compete for access [25], and in this case, the energy harvesting states reduce the number of devices contending for channel access thus improving throughput.

Next, we analyze the throughput of the network with different packet lengths  $L$ . By comparing Fig. 5.3(a) and Fig. 5.3(b), we observe that with the same number of nodes and the same energy harvesting rate, the network with longer packet length  $L$  has better throughput. When  $L$  becomes bigger, the value of  $E_{\min}$  increases, which means that the number of times a device attempts to transmit a packet before the energy harvesting process starts may decrease. But the simulation result shows that the length of a packet  $L$  has more influence than the value of  $E_{\min}$  on the network throughput.

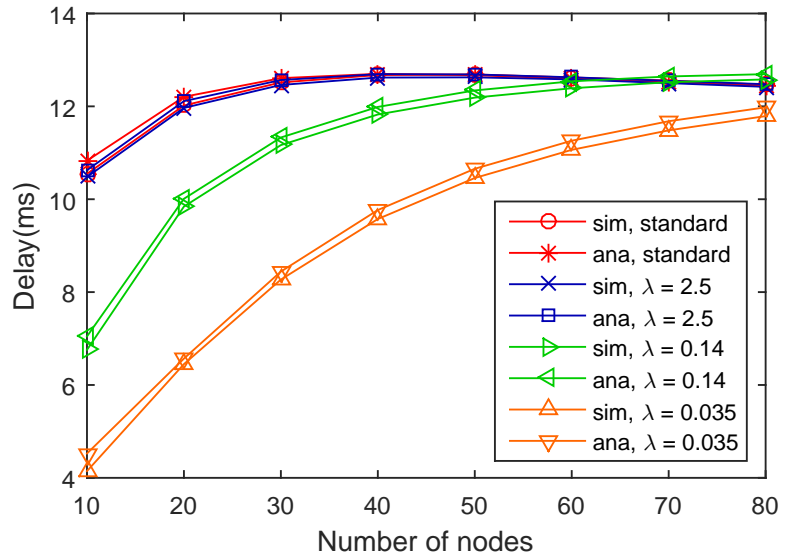
### 5.2.3 Delay

Figure 5.4 plots the average delay versus the number of nodes. The result of the analytical model tracks the simulation result well. We observe that (i) the average delay of the network without the energy constraint is higher than the network with energy harvesting sources, (ii) with the fixed number of nodes, the average delay decreases as the energy harvesting rate decreases, and (iii) with lower energy harvesting rate, the delay increases faster as the number of nodes increases. Those observations fully meet our expectation that the lower energy harvesting rate causes lesser channel contention, and reduces the channel usage. Similarly to the throughput result in Fig. 5.3, larger number of device can raise the channel contention, which causes longer waiting time to access the channel.

By comparing Fig. 5.4(a) and Fig. 5.4(b), it is clear that with the same energy harvest-

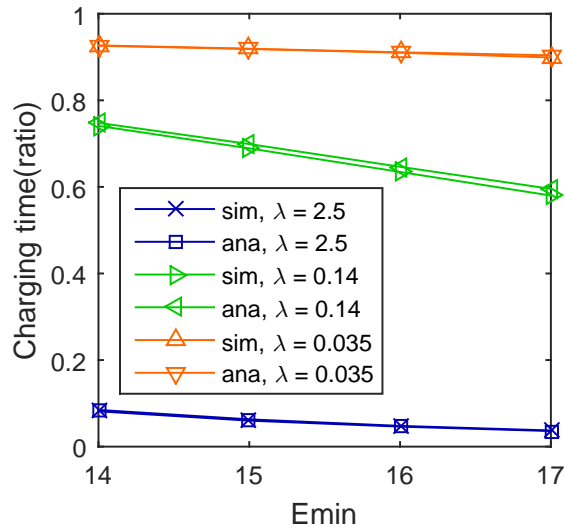


(a)  $E_{\min} = 16(L = 7)$

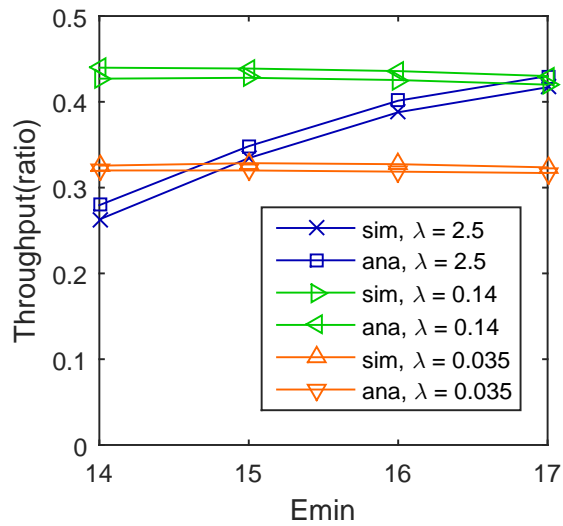


(b)  $E_{\min} = 11(L = 2)$

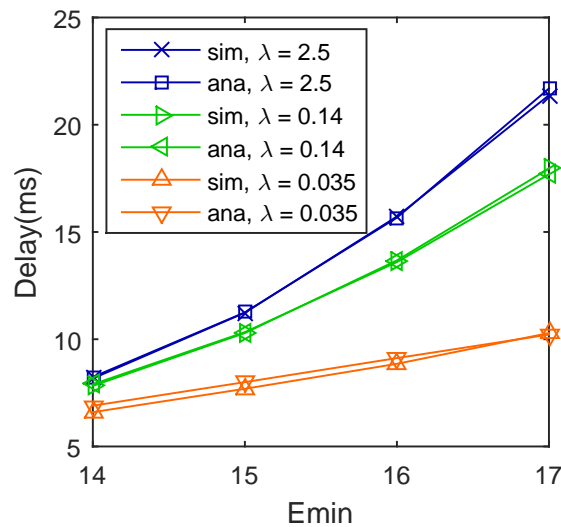
Figure 5.4: The average delay derived from the simulation(sim) and analytical model(ana) under different parameter setting. The parameter  $E_{\max} = 30$ ,  $q_0 = 0.3$ ,  $m_0 = 3$  and  $m = 4$



(a) Charging Time Ratio



(b) Throughput



(c) Delay

Figure 5.5: The performance with different value of  $E_{min}$  ( $m = 2, 3, 4, 5$ ). The parameter  $E_{max} = 30$ ,  $N = 20$ ,  $L = 7$ ,  $q_0 = 0.3$ , and  $m_0 = 3$

ing rate and the number of nodes, the larger packet lengths yields higher delay, and the delay is exaggerated when the number of nodes increase.



#### 5.2.4 $E_{\min}$ and $E_{\max}$

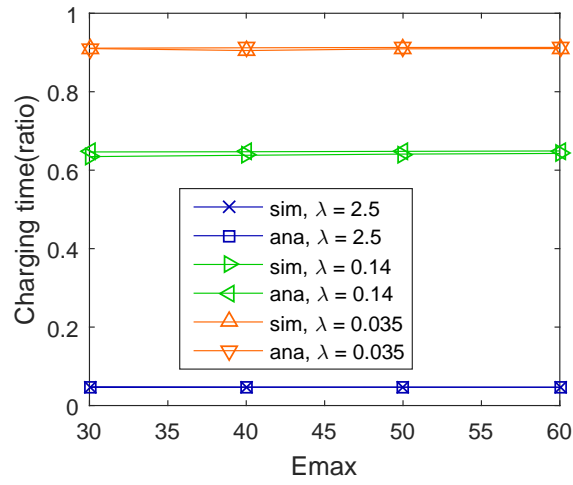
In this section, we seek to determine the network performance as a function of parameter  $E_{\min}$  and  $E_{\max}$ . In Fig. 5.5, we fix the value of packet size  $L$  and change the value of  $m$  (*macMAXCSMABackoffs*). With the larger number of  $m$ , the number of times that the device performs binary backoff for a packet can be increased. In Fig. 5.5(a), for  $\lambda = 0.035$ , because the channel usage is low, the device can easily access the channel when NB (number of backoffs) is small, which means that increasing the value of  $m$  has no effect on the charging time when the energy harvesting rate is small. For  $\lambda = 0.14$ , when  $m$  is increased, the device may spend more time on the binary backoff, so the average charging time is decreased. For  $\lambda = 2.5$ , since the average charging time with  $m = 2$  is small enough, the decrement of energy charging time is not very obvious when increasing  $m$ .

In Fig. 5.5(b), when  $N = 20$ , since only the network with  $\lambda = 2.5$  has optimized the channel usage, the throughput can be increased when we increase the value of  $m$ . In Fig. 5.5(c), larger  $m$  leads to the smaller probability that a packet is discarded due to the access failure, and more packets can be transmitted by increasing  $NB$ , but it will cause the larger average delay.

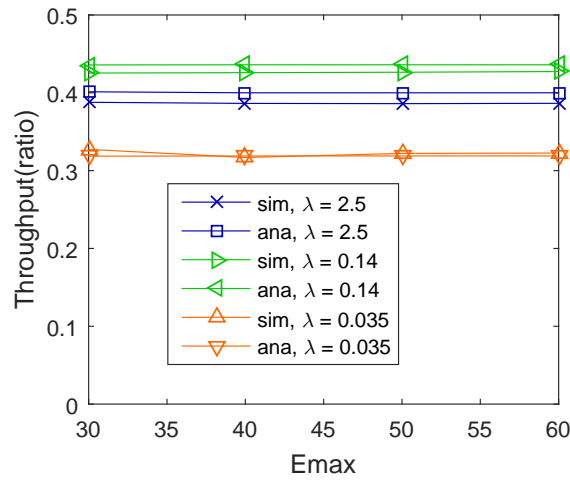
In Fig. 5.6, we seek to determine the network performance as a function of parameter  $E_{\max}$ . We compare the network charging time, throughput and delay with different energy harvesting rate and  $E_{\max} = 30, 40, 50$ , and  $60$ . We find that the performance difference is insignificant with increasing  $E_{\max}$ . Although larger  $E_{\max}$  can let a device work for longer time before entering the energy replenishing process, but the time staying in energy harvesting states is longer too. Hence, we conclude that  $E_{\max}$  is not an important factor on the network performance.

Based on the results presented in Figs. 5.2–5.6, we demonstrated that our Markov chain model successfully predicts the behavior of the slotted CSMA/CA protocol of IEEE

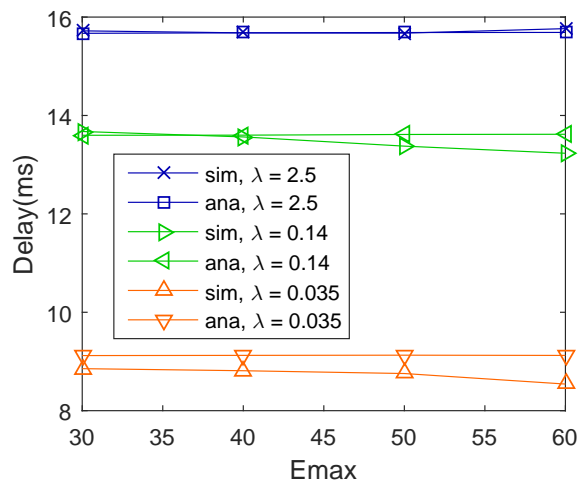




(a) Charging Time Ratio



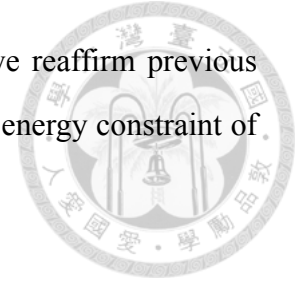
(b) Throughput



(c) Delay

Figure 5.6: The performance with different value of  $E_{max}$ . The parameter  $N = 20$ ,  $L = 7$ ,  $q_0 = 0.3$ ,  $m_0 = 3$  and  $m = 4$

802.15.4 standard with energy harvesting process. Additionally, we reaffirm previous findings [13] that the network performance is indeed different if the energy constraint of each device is considered.



# Chapter 6



## Conclusions

In this paper, we have analyzed the performance of the slotted CSMA/CA mechanism of the IEEE 802.15.4 standard taking into consideration the energy harvesting process in each IoT device. Insights to networked IoT performance with energy harvesting is expected to contribute to improving the prevailing energy constraints plaguing WSNs.

A Markov chain model is presented to analyze the performance of the slotted CSMA/CA mechanism with the energy harvesting process, and the performance is compared in terms of charging time, throughput and delay. The validity of the proposed model is proven by simulation. Analytical result shows that the performance of IoT devices with energy harvesting sources is different from typical CSMA/CA curves. We find that IoT devices with higher energy harvesting rate may have lower throughput if the network has large number of active nodes.

As the first attempt to incorporate energy harvesting process into the CSMA/CA mechanism for IEEE 802.15.4 standard, we make the assumption that the energy harvesting process follows the Poisson distribution and devices consume energy in discrete units. In practice, these assumptions may introduce errors into the predicted performance. Relaxing the above mentioned assumptions are immediate directions to improve the model and is left as the future work.

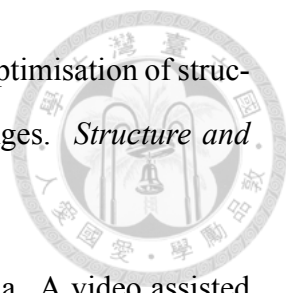
# Bibliography



- [1] Andrea Zanella, Nicola Bui, Angelo Castellani, and Lorenzo Vangelista and Michele Zorzi. Internet of things for smart cities. *IEEE Internet of Things Journal*, 1(1):22–32, 2014.
- [2] Winston K. G. Seah, Zhi Ang Eu, and Hwee-Pink Tan. Wireless Sensor Networks Powered by Ambient Energy Harvesting (WSN-HEAP) - Survey and Challenges. In *Proc. of the 1st International Conference on Wireless*, pages 1–5, 2009.
- [3] Z. Eu, H. Tan, and W. Seah. Design and performance analysis of MAC schemes for Wireless Sensor Networks Powered by Ambient Energy Harvesting. *Ad Hoc Networks*, 9(3):300–323, 2011.
- [4] Fabio Iannello, Osvaldo Simeone, and Umberto Spagnolini. Medium Access Control Protocols for Wireless Sensor Networks with Energy Harvesting. *IEEE Transactions on Communications*, 60(5):1381 – 1389, 2012.
- [5] T.R. Park, T. H. Choi, S. Choi, and W. H. Kwon. Throughput and energy consumption analysis of IEEE 802.15.4 slotted CSMA/CA. *Electronics Letters*, 41(18): 1017–1019, 2005.
- [6] Jelena Mišić, Vojislav B. Mišić, and Shairmina Shafi. Performance of a beacon enabled IEEE 802.15.4 cluster with downlink and uplink traffic. *IEEE Transactions on Parallel and Distributed Systems*, 17(4):361–376, 2006.
- [7] S. Pollin, M. Ergen, S. Ergen, B. Bougard, L. Der Perre, I. Moerman, A. Bahai, P. Varaiya, and F. Catthoor. Performance Analysis of Slotted Carrier Sense IEEE 802.15.4 Medium Access Layer. *IEEE Transactions on Wireless Communications*, 7(9):3359 – 3371, 2008.
- [8] P. Park, P. Di Marco, P. Soldati, C. Fischione, and K.H. Johansson. A generalized Markov chain model for effective analysis of slotted IEEE 802.15.4. In *Proc. of*

*IEEE 6th International Conference on Mobile Adhoc and Sensor Systems (MASS)*, pages 130–139, Macau, 12-15 Oct 2009.

- [9] Pangun Park, Carlo Fischione, and Karl Henrik Johansson. Modeling and Stability Analysis of Hybrid Multiple Access in the IEEE 802.15.4 Protocol. *ACM Transactions on Sensor Networks*, 9(2), 2013.
- [10] Giuseppe Bianchi. Performance Analysis of the IEEE 802.11 Distributed Coordination Function. *IEEE Journal on Selected Areas in Communications*, 18(3):535 – 547, 2000.
- [11] Jing Lei, Roy Yates, and Larry Greenstein. A Generic Model for Optimizing Single-Hop Transmission Policy of Replenishable Sensors. *IEEE Transactions on Wireless Communications*, 8(2), 2009.
- [12] Chin Keong Ho, Pham Dang Khoa, and Pang Chin Ming. Markovian Models for Harvested Energy in Wireless Communications. In *Proc. of IEEE International Conference on Communication Systems (ICCS)*, pages 311–315, 2010.
- [13] Ger Yang, Guan-Yu Lin, and Hung-Yu Wei. Markov Chain Performance Model for IEEE 802.11 Devices with Energy Harvesting Source. In *Proc. of Global Communications Conference (GLOBECOM)*, pages 5212–5217, 2012.
- [14] Nga Dang, Roberto Valentini, Eli Bozorgzadeh, Marco Levorato, and Nalini Venkatasubramanian. A Unified Stochastic Model for Energy Management in Solar-Powered Embedded Systems. In *Proc. of the IEEE/ACM International Conference on Computer-Aided Design (ICCAD)*, pages 621 – 626, 2015.
- [15] *IEEE Std 802.15.4-2011, September, Part 15.4: Low-Rate Wireless Personal Area Networks (LR-WPANs)*. IEEE, 2011.
- [16] A. Koubaa, M. Alves, and E. Tovar. A comprehensive simulation study of slotted CSMA/CA for IEEE 802.15.4 wireless sensor networks. In *Proc. of IEEE International Workshop on Factory Communication Systems*, pages 183–192, 28-30 June 2006.

- 
- [17] Dan M. Frangopol. Life-cycle performance, management, and optimisation of structural systems under uncertainty: accomplishments and challenges. *Structure and Infrastructure Engineering*, 7(6):389–413, 2011.
- [18] Yangbo Chen, Chin-An Tan, Maria Q. Feng, and Yoshio Fukuda. A video assisted approach for structural health monitoring of highway bridges under normal traffic. *Proc. SPIE*, 6174:1–18, 2006.
- [19] Ery Arias-Castro, Jan Kleissl, and Matthew Lave. A Poisson model for anisotropic solar ramp rate correlations . *Solar Energy*, 101:192–202, 2014.
- [20] Long Ren, Renwen Chen, Huakang Xia, and Xiaoxiao Zhang. Energy harvesting performance of a broadband electromagnetic vibration energy harvester for powering industrial wireless sensor networks. *proc. SPIE*, 9799:1–11, 2016.
- [21] Jinchu Han, Jun Hu, Yang Yang, Zhongxu Wang, Shan X. Wang, and Jinliang He. A nonintrusive power supply design for self-powered sensor networks in the smart-grid by scavenging energy from ac power line. *IEEE Transactions on Industrial Electronics*, 62(7):4398–4407, 2015.
- [22] Post, E. Rehmi, and Kit Waal. Electrostatic power harvesting for material computing. *Personal and Ubiquitous Computing*, 15(2):115–121, 2011.
- [23] Vladimir Leonov. Thermoelectric energy harvesting of human body heat for wearable sensors. *IEEE Sensors Journal*, 13(6):2284–2291, 2013.
- [24] NIWA. Solarview.
- [25] Jung Chang Yong, Hwang Ho Young, Sung Dan Keun, and Hwang Gang Uk. Enhanced Markov Chain Model and Throughput Analysis of the Slotted CSMA/CA for IEEE 802.15.4 Under Unsaturated Traffic Conditions. *IEEE Transactions on Vehicular Technology*, 58(1):473 – 478, 2009.